Available online at www.sciencedirect.com

ScienceDirect

Geochimica et Cosmochimica Acta 248 (2019) 123–137

Geochimica et Cosmochimica Acta

www.elsevier.com/locate/gca

The density of Li_2CO_3-Na_2CO_3-K_2CO_3-Rb_2CO_3-Cs_2CO_3-$CaCO_3$-$SrCO_3$-$BaCO_3$ liquids: New measurements, ideal mixing, and systematic trends with composition

Sean M. Hurt *, Rebecca A. Lange

Department of Earth and Environmental Sciences, University of Michigan, 2534 C.C. Little Bldg., 1100 N. University Ave., Ann Arbor, MI 48109-1005, USA

Received 19 October 2017; accepted in revised form 20 December 2018; available online 4 January 2019

Abstract

The densities of 15 liquids in the Li_2CO_3-Na_2CO_3-K_2CO_3-Rb_2CO_3-Cs_2CO_3-$CaCO_3$-$SrCO_3$-$BaCO_3$ system were measured at 1 bar with the Pt double-bob Archimedean method between 758 and 1455 K. Melt compositions contain ≤50 mol% $CaCO_3$, $SrCO_3$ and $BaCO_3$, and ≤100% Rb_2CO_3 and Cs_2CO_3. These results were combined with double-bob density measurements from the literature on nine liquids in the Li_2CO_3-Na_2CO_3-K_2CO_3-$CaCO_3$ system to calibrate a new linear volume equation for multicomponent carbonate liquids. The regression led to the following fitted partial molar volumes ($\pm 1\sigma$ cm^3/mol) at 1100 K for Li_2CO_3 (41.22 ± 0.09), Na_2CO_3 (53.27 ± 0.11), K_2CO_3 (71.59 ± 0.13), Rb_2CO_3 (80.78 ± 0.11), Cs_2CO_3 (94.00 ± 0.09), $CaCO_3$ (40.18 ± 0.16), $SrCO_3$ (44.33 ± 0.22) and $BaCO_3$ (50.99 ± 0.19). At 1100 K, the thermal expansion coefficients of all alkali carbonate liquid components are indistinguishable within 1-sigma error ($22.07 \pm 1.66 \times 10^{-5}$ K^{-1}), but differ from the thermal expansion coefficients of all alkaline-earth carbonate liquid components, which are also indistinguishable within 1-sigma error ($16.40 \pm 2.85 \times 10^{-5}$ K^{-1}). The linear volume equation recovers the measurements within analytical error (±0.3%). The partial molar volumes of all eight carbonate components increase linearly along two different trends, one for the alkali carbonates ($R^2 = 0.999$) and another for the alkaline earth carbonates ($R^2 = 0.999$) as a function of cation volumes, where metal cation-oxygen coordination numbers are obtained from molecular dynamic simulations in the literature (ranging from 4- to 6-fold among the alkali metals and 7- to 8-fold among the alkaline-earth metals). The linear fits lead to two different partial molar volumes (~38 and ~31 cm^3/mole) for the carbonate ion (CO_3^{2-}) at 1100 K, which reflects a more open topological arrangement of the carbonate ions when in 4-fold coordination with the alkali metals vs. 6-fold coordination with alkaline earth metals. The results permit the partial molar volume of $MgCO_3$ and $FeCO_3$ in multicomponent carbonate liquids to be calculated if the oxygen and carbonate ion coordination with Mg^{2+} and Fe^{2+} are known. For example, in the case where Mg^{2+} and Fe^{2+} are in 6-fold coordination with both oxygen and carbonate, the estimated partial molar volumes at 1100 K are 34.4 (±0.6), and 35.1 (±0.6) cm^3/mol, respectively, with a thermal expansion coefficient of 16.40 (±2.85) 10^{-5} K^{-1}. In contrast, if Mg^{2+} and Fe^{2+} are in 4-fold coordination with both oxygen and carbonate, the estimated partial molar volumes at 1100 K are 40.0 (±0.6), and 40.4 (±0.6) cm^3/mol, respectively, with a thermal expansion coefficient of 22.07 (±1.66) 10^{-5} K^{-1}. To resolve these different estimates of molar volume, molecular dynamic simulations are needed to determine the respective coordination environments for Mg^{2+} and Fe^{2+} in carbonate liquids.

* Corresponding author.
E-mail address: seanhurt@umich.edu (S.M. Hurt).

https://doi.org/10.1016/j.gca.2018.12.031
0016-7037/

1. INTRODUCTION

Despite its relatively low abundance in the mantle, carbonate plays a key role in the global carbon cycle and in the formation of mantle melts in various tectonic settings (e.g., Dasgupta and Hirschmann, 2010). Carbonate may be a major factor in deep (240–300 km) partial melting of the mantle beneath mid-ocean spreading ridges and intraplate settings (e.g., Dasgupta and Hirschmann, 2006), and it plays a critical role in the genesis of silica-undersaturated alkaline magmas (e.g., Dasgupta et al., 2006). Moreover, because carbonate melts are efficient scavengers of various incompatible elements (e.g., Blundy and Dalton, 2000), they are also effective agents of mantle metasomatism (e.g., Dalton and Wood, 1993). Therefore, understanding the stability of carbonate melts under mantle conditions and incorporating them into thermodynamic models (e.g., p-MELTS; Ghiorso et al., 2002) is a major imperative. In order to extend thermodynamic models to include carbonate melts it is necessary to constrain their equation of state (P-V-T relation). The objective of this study is to expand the compositional range of carbonate liquids for which direct density measurements are known at 1-bar, with a focus on alkaline-earth components.

The three most abundant carbonate components in the mantle are $MgCO_3$, $CaCO_3$ and $FeCO_3$; however these three pure end-member liquids are not stable at one bar and decompose at temperatures below their melting temperatures. In previous studies, Liu and Lange (2003) and O'Leary et al. (2015) showed that the $CaCO_3$ component could be added to low-temperature alkali carbonate liquids to form $CaCO_3$-bearing liquids that are stable at one bar. The same strategy was employed in this study, where $CaCO_3$, $SrCO_3$, and $BaCO_3$ were added in various proportions ($\leq$50 mol%) to the eutectic in the Li_2CO_3-Na_2CO_3-K_2CO_3 ternary to permit density measurements of alkaline earth carbonate-bearing liquids to be obtained over as wide a range of composition and temperature as possible. In addition, the density of melts with 50–100% Rb_2CO_3 and Cs_2CO_3 were also measured. By expanding the compositional data set for which double-bob liquid density measurements are currently available from four to eight components (Li_2CO_3-Na_2CO_3-K_2CO_3-Rb_2CO_3-$Cs_2CO_3$$CaCO_3$-$SrCO_3$-$BaCO_3$), systematic variations with composition and temperature can be evaluated. This in turn allows constraints to be placed on the partial molar volume and thermal expansion of the $MgCO_3$ and $FeCO_3$ components in multicomponent carbonate liquids at 1 bar. Standard state thermodynamic property estimates on these critical components are necessary to extend thermodynamic models such as p-MELTS to carbonated-bearing lithologies relevant to the mantle.

2. MATERIALS AND METHODS

2.1. Sample synthesis

Fifteen samples in the Li_2CO_3-Na_2CO_3-K_2CO_3-Rb_2CO_3-Cs_2CO_3-$CaCO_3$-$SrCO_3$-$BaCO_3$ system were synthesized in this study (Table 1). For 13 of these samples, the eutectic composition in the Li_2CO_3-Na_2CO_3-K_2CO_3 ternary (referred to as T in Table 1) was combined with varying amounts of $CaCO_3$, $SrCO_3$, $BaCO_3$, Cs_2CO_3 and Rb_2CO_3. The remaining two samples are pure Rb_2CO_3 and Cs_2CO_3. The samples were made in 200 g batches from powdered or granular reagents with >99.5% purity. Before synthesis, the loss on ignition (LOI) of each reagent was determined and used to calculate the appropriate weight of each reagent to be poured directly into the glass jar of an electric blender. The reagents were mixed at high speeds for several minutes to make a powdered sample with a homogenous composition.

2.2. Double-bob Archimedean method

The double-bob Archimedean method was used to determine the density of each experimental liquid over a 697° temperature interval (758–1455 K), following the methods described in detail in Lange and Carmichael (1987) and Liu and Lange (2003). Sufficient amounts of each sample ($\sim$75 g) were loaded into a Pt crucible to ensure a liquid depth of $\sim$2.5 cm. The sample and Pt crucible were loaded into a Deltech vertical tube furnace and brought up to temperature under a constant stream of pure CO_2 gas.

Table 1
Molar composition and gram formula weight (g.f.w.) of experimental liquids.

Sample	Li_2CO_3	Na_2CO_3	K_2CO_3	Rb_2CO_3	Cs_2CO_3	$CaCO_3$	$SrCO_3$	$BaCO_3$	g.f.w.
T-50%Rb				0.500					124.22
Rb_2CO_3				1.000					230.95
T-50%Cs	0.218	0.158	0.125		0.500				212.95
Cs_2CO_3					1.000				325.82
T-25% Ca	0.326	0.236	0.188			0.250			100.08
T-35%Ca	0.283	0.205	0.163			0.350			100.08
T-50%Ca	0.218	0.158	0.125			0.500			100.08
T-10%Sr	0.392	0.284	0.225				0.100		104.84
T-20%Sr	0.348	0.252	0.200				0.200		109.59
T-30%Sr	0.305	0.221	0.175				0.300		114.35
T-50%Sr	0.218	0.158	0.125				0.500		123.79
T-15%Ba	0.370	0.268	0.213					0.150	114.67
T-35%Ba	0.283	0.205	0.163					0.350	134.12
T-50%Ba	0.218	0.158	0.125					0.500	148.71
T-50%CaSrBa	0.218	0.158	0.125			0.167	0.167	0.167	111.26

A density measurement was made by suspending a Pt bob from a mass balance (with a precision of ±0.0001 g) above the surface of the sample liquid. The bob and sample were allowed at least thirty minutes to come to thermal equilibrium. The bob was weighed and then immersed in the sample liquid and weighed again to obtain buoyancy, $B(T)$. The density of the liquid is obtained from the relation:

$$\rho^{liq}(T) = \frac{B(T) + S(T)}{V(T)} \quad (1)$$

where $\rho^{liq}(T)$ is the density of the liquid at the experimental temperature, $B(T)$ is the buoyancy, $S(T)$ is the surface tension effect from the liquid surface pulling on the stem of the bob, and $V(T)$ is the volume of the bob immersed in the liquid. The procedure was repeated with a second bob of different size, which allows the $S(T)$ term to be eliminated in the calculation of density with the following equation:

$$\rho^{liq}(T) = \frac{B_L(T) - B_S(T)}{V_L(T) - V_S(T)} \quad (2)$$

where the L and S subscripts denote a large and small bob, respectively. The buoyancy measurements were repeated with two different large bobs (26.4 and 25.9 g) and two different small bobs (11.7 and 9.8 g), which allowed four different density measurements to be obtained at each experimental temperature, using Eq. (2). To further assess reproducibility, replicate density measurements were made on two different aliquots from the same synthesized sample batch in two cases (T-10%Sr and T-50%Ba), and the T-35%Ba sample was re-synthesized from scratch and its density re-measured. The $BaCO_3$-bearing liquids posed experimental difficulties not found for the other sample liquids, where the platinum bobs were prone to adhering to the sides of the crucible as they were immersed during a buoyancy measurement.

Density measurements were made at three to four different temperatures, with the temperature interval bounded by the liquidus and decomposition temperature of each sample. For one sample (T-35%Ca; Table 1), liquid density was measured at only one temperature because the supply of CO_2 ran out and there was insufficient CO_2 in the furnace tube to prevent decarbonation (decomposition) of the sample. For the alkaline earth carbonate components, measurements were made over temperature intervals that ranged from 444 ($CaCO_3$), 697 ($SrCO_3$) and 407 ($BaCO_3$) K. For the Rb_2CO_3 and Cs_2CO_3 components, density measurements were made over temperature intervals of 392 and 355 K, respectively.

2.2.1. Temperature control

Determination of the experimental temperature during each density measurement was obtained with the following calibration. The Pt crucible was filled with alumina (Al_2O_3) powder to the same depth as that used for the experimental liquids and placed in the furnace. A thermocouple was buried two cm deep into the powder, a depth corresponding to that of immersed bobs, and the recorded temperature was used to locate the furnace hotspot and isothermal zone. The crucible was situated so that the sample was near the bottom of the isothermal zone to ensure that the liquid at the bottom of the crucible was not hotter than the top, which prevented convection. The furnace was then set to various temperatures, spanning the range used in the density experiments (800–1500 K). The thermocouple temperature was recorded at each set point and used to create a temperature calibration curve. The thermocouple used in temperature calibration was also tested for accuracy against the melting point of gold; the gold melted within five degrees of the accepted value (1337 K).

2.2.2. Density measurements of liquid NaCl as a standard

To verify the accuracy of the Pt double-bob Archimedean method and the temperature calibration curve employed in this study, the density of liquid NaCl was measured eleven different times between 1102 and 1455 K. These measurements were made before, during and after the density measurements on the sample liquids in Table 1 were made.

3. RESULTS

3.1. NaCl liquid density

The NaCl liquid density results are listed in Table 2 at each temperature of measurement, together with molar volume, which is calculated by dividing the molar mass of NaCl (58.44 g/mol) by density. In Fig. 1, the liquid molar volume data from this study are plotted against temperature and compared to those reported in Stein et al. (1986), Lange and Carmichael (1987), Liu and Lange (2001, 2006) and Guo et al. (2013), all of which are based on the double-bob Archimedean method. The results from this study expand the temperature interval for which density data are available for NaCl liquid from 194 to 353°, which improves estimates of its thermal expansion. A linear fit to the data in Fig. 1 gives the molar volume of NaCl liquid as a function of temperature: $V(T) = 22.11 + 0.0143 \cdot T$ (K) cm^3/mol. This linear fit recovers the measurements from the literature within 0.35%, on average, and those from this study within 0.25%, on average.

3.2. Carbonate liquid densities

The density results for the 15 experimental liquids at each temperature of measurement are reported in Table 3.

Table 2
NaCl liquid density measurements.

Temp. (K)	Density (g/cm^3)	Volume (cm^3/mol)
1102	1.535	38.07
1102	1.540	37.95
1152	1.513	38.63
1152	1.516	38.55
1152	1.516	38.55
1204	1.488	39.28
1244	1.467	39.84
1310	1.429	40.88
1360	1.399	41.79
1455	1.364	42.86
1455	1.372	42.60

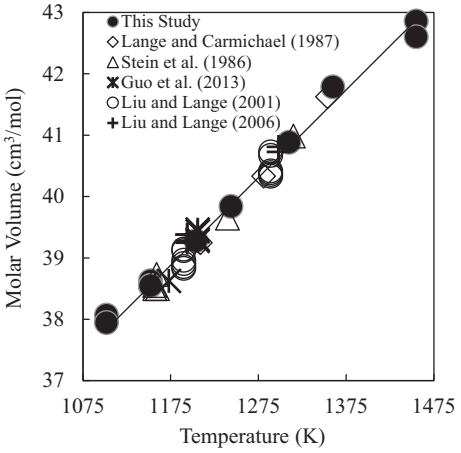

Fig. 1. Liquid NaCl molar volume data with temperature from this study and other double-bob Archimedean results from the literature.

Molar volumes were calculated by dividing the measured density into the gram formula weight (g.f.w.; defined in Table 1) of each sample. Molar volumes of all liquids are plotted as a function of temperature in Fig. 2. Ideally, each density result at each temperature should be based on the average of four (n = 4; Table 3) density determinations obtained from four bobs (two large and two small). However, during some experiments, one or two of the four bob measurements failed, often because the bob adhered to the crucible wall during immersion. In some cases, many more bob buoyancy measurements were made, enabling more density determinations, and in Table 3, the number of different density measurements at each experimental temperature ranges from one to 13. The standard deviation of the measured density for each sample ranges from 0.04 to 0.57%, and the average is 0.26%, which is identical to the measurement error of Liu and Lange (2003).

A linear fit of the molar volume with temperature was made for each sample liquid with the following equation:

$$V(T) = a_{1100\mathrm{K}} + b(T - 1100\ \mathrm{K}) \quad (3)$$

where $V(T)$ is the molar volume of the liquid, a is the fitted molar volume of the liquid at 1100 K, b is the thermal expansivity $\frac{\delta V}{\delta T}$ and T is temperature in Kelvin. Table 4 gives the fitted values of a and b for all sample liquids (except T-35%Ca, for which molar volume was obtained at only one temperature; Table 3).

3.3. A linear model equation for molar volume

The molar volume data for the 15 liquids in Table 3 were combined with those from Liu and Lange (2003) on nine Li_2CO_3-Na_2CO_3-K_2CO_3-$CaCO_3$ liquids in a fit to the following linear volume equation:

$$V^{liq}(X,T) = \sum X_i \left(\bar{V}_{i,1100\mathrm{K}} + \frac{\delta \bar{V}_i}{\delta T}[T - 1100\ \mathrm{K}] \right). \quad (4)$$

In Eq. (4), V^{liq} is the measured molar volume, X_i is the mole fraction of each carbonate component i in each experimental liquid, $\bar{V}_{i,1100\mathrm{K}}$ is the partial molar volume of each carbonate component at 1100 K, and $\frac{\delta \bar{V}_i}{\delta T}$ is the partial molar thermal expansivity of each carbonate component. Fitted values of $\bar{V}_i$ and $\frac{\delta \bar{V}_i}{\delta T}$ for each carbonate component were obtained by multiple linear regression of Eq. (4) and reported in Table 5. The final adjusted R^2 of the fit is 0.98. The average residual is ±0.32%, which is close to the average analytical error for density of 0.26%. Most importantly, the residuals show no systematic variation with temperature (Fig. 3) or composition (Fig. 4). The maximum residual of 0.89% is for a $BaCO_3$-bearing liquid, which is not surprising given the experimental challenges with these liquids. The results from this study show that the molar volume of multicomponent carbonate liquids, including those with more than one alkaline earth carbonate component (e.g, T-50CaSrBa; Table 1), mix ideally with respect to composition in the Li_2CO_3-Na_2CO_3-K_2CO_3-Rb_2CO_3-$CaCO_3$-$SrCO_3$-$BaCO_3$ system. Moreover, for the alkali carbonate components, (Rb_2CO_3 and Cs_2CO_3 in this study; Li_2CO_3, Na_2CO_3 and K_2CO_3 in Liu and Lange, 2003), the fitted partial molar volumes (Table 5) match those for the pure end-members (Table 4).

3.4. Constant thermal expansion coefficients for alkali vs. alkaline earth carbonate liquids

A plot of the thermal expansion coefficient, $\alpha = \left(1/\bar{V}_i\right)/\left(\partial \bar{V}_i/\partial T\right)$, for each liquid carbonate component at 1100 K is shown in Fig. 5 as a function of cation volume. The thermal expansion coefficient appears to be independent of composition, within error, among all five alkali carbonate liquids, with an average value of 22.5 (±2.1) 10^{-5} K^{-1}, and among all three alkaline earth carbonate liquid components, with an average value of 16.4 (±2.3) 10^{-5} K^{-1}.

3.5. Comparison to results based on the maximum bubble pressure method

The liquid density results from this study are compared to those on Li_2CO_3-Na_2CO_3-K_2CO_3-Rb_2CO_3-Cs_2CO_3-$CaCO_3$-$SrCO_3$-$BaCO_3$ liquids from the literature based on the maximum bubble pressure technique (Kojima et al., 1999, 2003, 2008), with a reported error of 0.9%. Although the Kojima et al. density measurements were made on carbonate liquids in the same eight-component system, only two compositions from those three studies match those from this study, namely pure Rb_2CO_3 and Cs_2CO_3. A direct comparison of the density results is made in Fig. 6; there is general agreement for Rb_2CO_3 liquid, but the density results for Cs_2CO_3 liquid from this study are ~1.8% higher than those measured by Kojima et al. (1999).

A global comparison of all the density results on the eight-component carbonate liquids from the maximum bubble pressure method, converted to molar volume, to those from the double-bob Archimedean method is made

Table 3
Experimental liquid density measurements and molar volumes.

Sample	Temp (K)	ρ (g/cm^3)	[a]SD	[b]N	$V_{meas.}$ (cm^3/g.f.w.)	[c]$V_{calc.}$ (cm^3/g.f.w.)	[d]% diff (meas-calc)
T-25%Ca	813	2.138	0.30	4	46.81	46.52	0.63
T-25%Ca	859	2.123	0.23	4	47.14	47.00	0.31
T-25%Ca	912	2.112	0.30	4	47.39	47.54	−0.32
T-25%Ca	1152	1.992	0.17	4	50.24	50.05	0.39
T-25%Ca	1257	1.948	0.25	4	51.38	51.14	0.47
T-35%Ca	1007	2.110	0.43	4	47.43	47.34	0.20
T-50%Ca	1007	2.201	0.21	2	45.47	45.54	−0.16
T-50%Ca	1054	2.181	0.13	4	45.89	45.98	−0.19
T-50%Ca	1102	2.164	0.25	1	46.25	46.42	−0.36
T-10%Sr	758	2.170	0.08	4	48.31	47.98	0.69
T-10%Sr	859	2.123	0.31	2	49.38	49.11	0.55
T-10%Sr	1257	1.966	0.29	10	53.32	53.52	−0.37
T-20%Sr	1102	2.141	0.16	2	51.19	50.98	0.41
T-20%Sr	1257	2.071	0.30	4	52.92	52.61	0.58
T-20%Sr	1455	2.002	0.20	4	54.74	54.71	0.05
T-30%Sr	960	2.351	0.31	4	48.64	48.72	−0.17
T-30%Sr	1054	2.305	0.42	4	49.61	49.66	−0.12
T-30%Sr	1152	2.248	0.32	2	50.87	50.65	0.42
T-50%Sr	1152	2.524	0.29	2	49.04	48.97	0.15
T-50%Sr	1152	2.540	0.10	4	48.74	48.97	−0.48
T-50%Sr	1257	2.489	0.17	4	49.73	49.91	−0.36
T-50%Sr	1362	2.433	0.47	4	50.88	50.87	0.02
T-50%Sr	1455	2.390	0.09	4	51.79	51.71	0.17
T-15%Ba	850	2.316	0.16	4	49.51	49.56	−0.11
T-15%Ba	960	2.253	0.36	4	50.90	50.80	0.18
T-35%Ba	960	2.643	0.24	7	50.75	50.56	0.36
T-35%Ba	1102	2.553	0.46	7	52.53	52.07	0.89
T-35%Ba	1152	2.546	0.57	13	52.68	52.60	0.15
T-35%Ba	1204	2.534	0.24	4	52.93	53.14	−0.41
T-35%Ba	1257	2.503	0.56	4	53.58	53.70	−0.22
T-50%Ba	1102	2.887	0.05	4	51.51	51.83	−0.61
T-50%Ba	1127	2.852	0.47	4	52.14	52.08	0.13
T-50%Ba	1152	2.855	0.07	2	52.09	52.33	−0.47
T-50%Ba	1257	2.769	0.08	4	53.71	53.39	0.59
T-50%Rb	865	2.618	0.08	4	63.22	63.22	0.01
T-50%Rb	885	2.621	0.32	4	63.15	63.51	−0.57
T-50%Rb	982	2.537	0.17	4	65.24	64.95	0.45
T-50%Rb	1078	2.491	0.07	4	66.44	66.37	0.11
T-50%Rb	1152	2.453	0.42	4	67.47	67.47	0.01
T-50%Rb	1112	2.476	0.20	4	66.85	66.87	−0.04
Rb_2CO_3	1152	2.819	0.23	2	81.92	81.72	0.25
Rb_2CO_3	1257	2.769	0.23	3	83.40	83.60	−0.24
T-50%CaSrBa	1030	2.587	0.20	4	48.02	48.23	−0.44
T-50%CaSrBa	1080	2.556	0.00	1	48.60	48.70	−0.21
T-50%Cs	859	3.085	0.45	4	69.03	69.22	−0.28
T-50%Cs	960	3.009	0.56	4	70.77	70.93	−0.23
T-50%Cs	1112	2.881	0.54	2	73.92	73.51	0.55
Cs_2CO_3	1112	3.461	0.07	4	94.14	94.27	−0.14
Cs_2CO_3	1122	3.438	0.30	4	94.77	94.49	0.29
Cs_2CO_3	1127	3.433	0.39	4	94.91	94.60	0.32
Cs_2CO_3	1163	3.419	0.21	4	95.30	95.41	−0.11
Cs_2CO_3	1214	3.388	0.04	4	96.17	96.54	−0.39

[a] SD = 1 − sigma standard deviation (%) on each density determination.
[b] N = number of separate density measurements.
[c] Vcalc = calculated from Eq. (4) and fitted terms in Table 5.
[d] % diff = 100 * (Vmeas − Vcalc)/Vmeas.

by comparing the results of a fit to the model equation in Eq. (4). In Table 6, the fitted values for the partial molar volume and thermal expansivity of each of the carbonate components, based on the density data from Kojima et al. (1999, 2003, 2008), are shown. A comparison of the results in Tables 5 and 6 shows that the largest differences are seen for the alkaline earth carbonate components, where the errors on the fitted terms based on the maximum bubble pressure method (Table 6) are larger by a factor of two than those based on the double-bob method (Table 5).

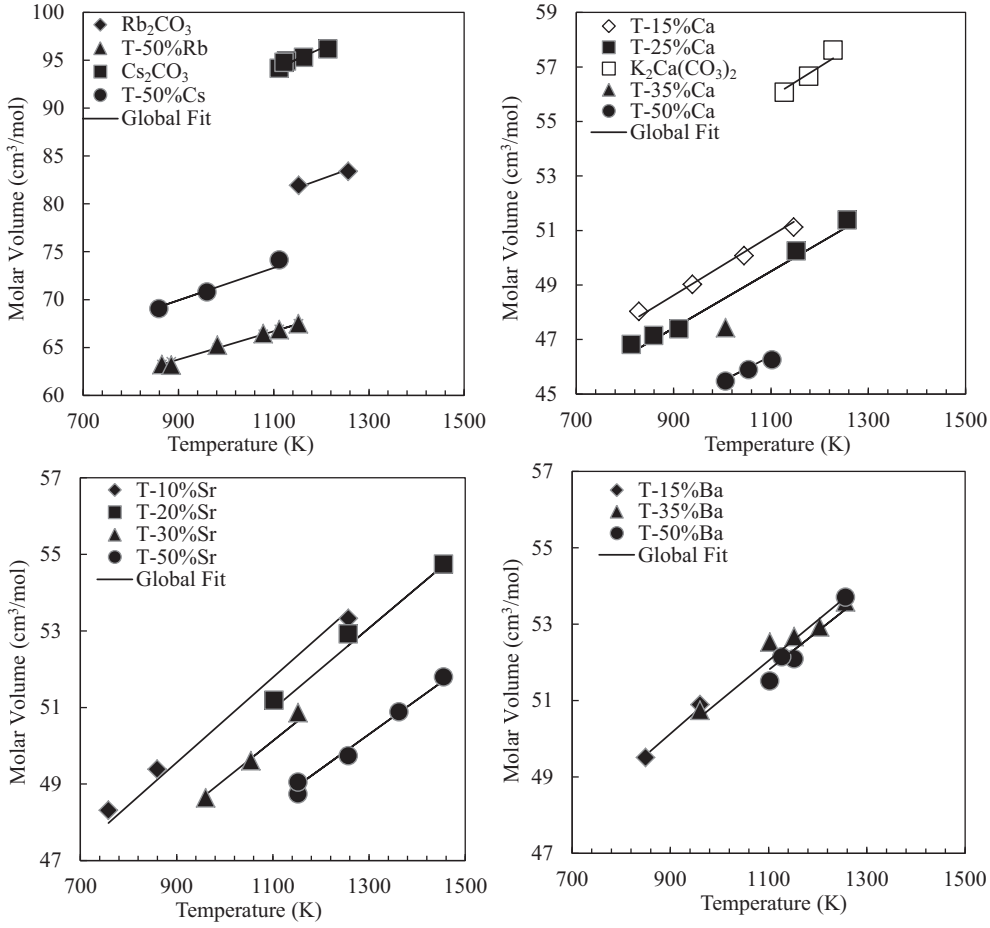

Fig. 2. Molar volumes of experimental liquids with temperature from this study (solid symbols) and Liu and Lange (2003) (open symbols). The lines are the global fit to the entire data set (Eq. (4) and Table 5).

Table 4
Linear fit to volume of each experimental liquid.

$V = a_{1100K} + b(T - 1100\ \mathrm{K})$ cm^3/g.f.w.			
Sample	a_{1100K}	$b{\cdot}10^3$	Temp. range (K)
T-25%Ca	49.67	10.62	813–1257
T-35%Ca	–	–	1007
T-50%Ca	46.24	8.16	1007–1102
T-10%Sr	51.76	10.01	758–1257
T-20%Sr	51.23	10.04	1102–1455
T-30%Sr	50.22	11.61	960–1152
T-50%Sr	48.35	9.61	1152–1455
T-15%Ba	52.64	12.50	850–960
T-35%Ba	52.17	9.13	960–1257
T-50%Ba	51.55	13.63	1102–1257
T-50%Rb	66.74	15.36	1152–1257
Rb_2CO_3	81.18	14.16	865–1152
T-50%CaSrBa	48.83	11.65	1030–1080
T-50%Cs	73.63	19.43	859–1112
Cs_2CO_3	94.24	17.24	1112–1214

Table 5
Fitted partial molar volumes (Eq. (4)).

$V = V_{i(1100K)} + \delta V_i/\delta T\ (T - 1100\ \mathrm{K})$		
Component	$V_{i(1100K)}$ (cm^3/mol)	$\delta V_i/\delta T$ (10^{-3} cm^3/mol K)
Li_2CO_3	41.22 ± 0.09	8.83 ± 1.20
Na_2CO_3	53.27 ± 0.11	12.30 ± 1.11
K_2CO_3	71.59 ± 0.13	15.68 ± 1.13
Rb_2CO_3	80.78 ± 0.11	17.98 ± 0.90
Cs_2CO_3	94.00 ± 0.09	22.28 ± 1.14
$CaCO_3$	40.18 ± 0.16	6.75 ± 1.52
$SrCO_3$	44.33 ± 0.22	6.40 ± 1.20
$BaCO_3$	50.99 ± 0.19	8.65 ± 1.90

Calibration data set: this study and Liu and Lange (2003).

This is consistent with the larger error on density for the maximum bubble pressure method (~0.9%; Kojima et al., 1999, 2003, 2008) compared to that for the double-bob method (~0.3%; Liu and Lange, 2003; this study). Therefore, although the two sets of density measurements obtained by different techniques are broadly consistent, they were not combined into a final data set. The recommended values to use in the molar volume equation (Eq. (4)) are those in Table 5 and based solely on Pt double-bob Archimedean density measurements.

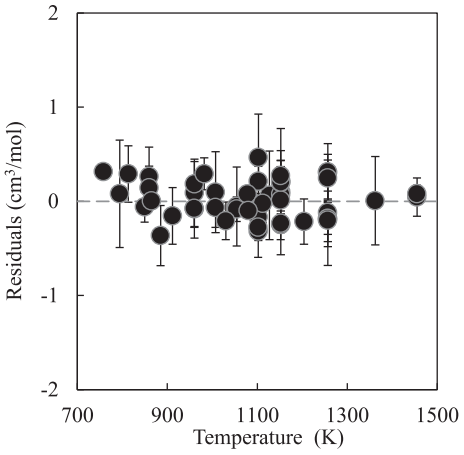

Fig. 3. Residuals from fit to Eq. (4) as a function of temperature. Two-sigma error bars are shown.

4. DISCUSSION

4.1. A comparison of crystalline and liquid molar volumes with temperature

The newly calibrated volume equation (Eq. (4)), with the fitted parameters in Table 5, can be used to calculate the molar volume of each liquid carbonate component with temperature and compare it to their crystalline molar volume with temperature, for phases where these data are available from X-ray and neutron diffraction studies. This allows a direct comparison to be made between crystal and liquid volumes over a range of temperatures, and it shows how changes in crystal structure and cation coordination affect molar volumes. In Table 7, crystalline volumes for each of the eight carbonates (and their polymorphs) at both 298 and 1100 K have been collected from the literature and compared to their respective liquid volumes at 1100 K.

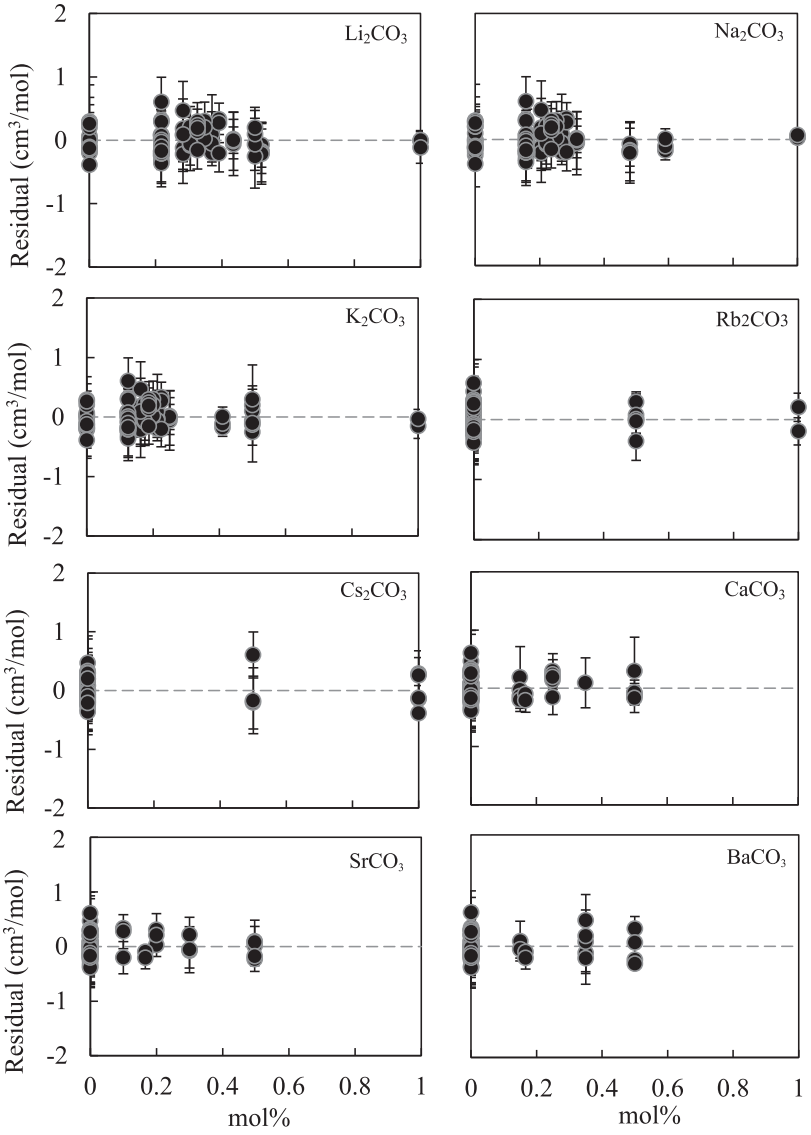

Fig. 4. Residuals from fit to Eq. (4) as a function of composition. Two-sigma error bars are shown.

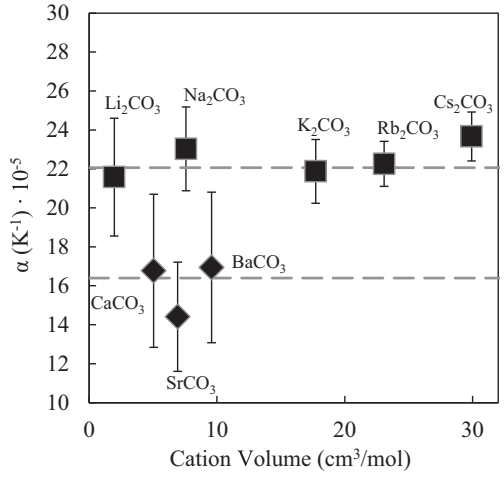

Fig. 5. Thermal expansion coefficient derived for each carbonate liquid component at 1100 K versus cation volume. Dashed lines are average for alkali carbonate liquids ($22.07 \cdot 10^{-5}$ K^{-1}) and the alkaline earth carbonate liquids ($16.40 \cdot 10^{-5}$ K^{-1}).

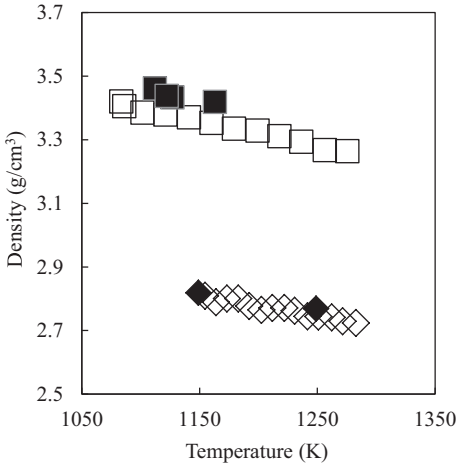

Fig. 6. Liquid density measurements for Rb_2CO_3 (diamonds) and Cs_2CO_3 (squares) with temperature (solid symbols, this study; open symbols, Kojima et al., 1999).

Table 6
Fit of Eq. (4) on data from Kojima et al. (1999, 2003, 2008).

$V = V_{i(1100K)} + \delta V_i/\delta T\,(T - 1100\ K)$		
Component	$V_{i(1100K)}$ (cm^3/mol)	$\delta V_i/\delta T$ (10^{-3} cm^3/mol K)
Li_2CO_3	41.58 ± 0.11	8.41 ± 0.83
Na_2CO_3	53.25 ± 0.14	12.48 ± 1.14
K_2CO_3	72.01 ± 0.22	16.55 ± 1.53
Rb_2CO_3	81.47 ± 0.17	19.33 ± 1.22
Cs_2CO_3	95.69 ± 0.17	22.61 ± 1.17
$CaCO_3$	39.14 ± 0.40	7.35 ± 3.41
$SrCO_3$	43.12 ± 0.39	11.84 ± 3.84
$BaCO_3$	48.40 ± 0.40	9.09 ± 3.34

For crystalline Li_2CO_3, a volume equation from Liu and Lange (2003) (citing data from A. Kirfel and B. Barbier) has been used (T is in Celsius):

$$V(T)_{Li2CO3} = 35.2804 + 1.510 \times 10^{-3} T + 1.440 \times 10^{-6} T^2 \quad cm^3/mol \tag{5}$$

Among the alkali carbonates, a comparison of crystalline volumes at 298 K to the liquid at 1100 K reveals a systematic decrease in the liquid to crystal volume ratio (V_{liq}/V_{xtl}) from Na_2CO_3 (1.28) to Cs_2CO_3 (1.22); the exception to this trend is Li_2CO_3 with a V_{liq}/V_{xtl} ratio of 1.17. Among the alkaline earth carbonates, the similar trend is observed for the orthorhombic *Pmcn* phases, namely a systematic decline in V_{liq}/V_{xtl} from $CaCO_3$ (1.18) to $BaCO_3$ (1.12).

At 1100 K, the crystalline alkali carbonates have all transitioned to a hexagonal structure (usually $P6_3/mmc$) and in all cases the V_{liq}/V_{xtl} ratio is ~1.10. For $CaCO_3$, $SrCO_3$ and $BaCO_3$, the $R3m$ or $R\bar{3}m$ phases are stable near 1100 K. $CaCO_3$ undergoes a phase transition from $R\bar{3}c$ to $R\bar{3}m$ at ~1240 K (e.g. Antao and Hassan, 2009; Ishizawa et al., 2013) whereas $SrCO_3$ and $BaCO_3$ undergo a phase change to a hexagonal structure ($R3m$ or $R\bar{3}m$ at ~1173 and ~1073 K, respectively. The orthorhombic to hexagonal phase change is accompanied by a marked increase in volume (4.7%, 3.8% and 2.7% for $CaCO_3$, $SrCO_3$ and $BaCO_3$, respectively). The alkaline earth carbonates range to lower V_{liq}/V_{xtl} ratios at 1100 K (≥1.04) than the 1.10 ratio for all the alkali carbonates. This suggests that the hexagonal alkaline earth carbonate structures (i.e. $R3m$ or $R\bar{3}m$) are more similar to the average liquid structure than are the hexagonal alkali carbonate structures (i.e. $P6_3/mmc$).

Using the General Lattice Utility Program (Gale and Rohl, 2003), pair distribution functions (Cope and Dove, 2007) were calculated in this study for a subset of the crystalline structures for Li_2CO_3, Na_2CO_3, K_2CO_3, $CaCO_3$ and $BaCO_3$. The objective was to obtain coordination numbers for carbonate-carbonate (C-C), metal cation-carbonate (M-C) and metal cation-oxygen (M-O) pairs. These coordination numbers are listed in Table 8 and compared with those calculated for the respective liquid carbonates (Tissen and Janssen, 1990; Vuilleumier et al., 2014).

The coordination of the metal cation with both oxygen and carbonate for all eight crystalline structures are similar to those for the corresponding liquids (Table 8). Instead, the primary structural difference between the crystals and the corresponding liquids is in the carbonate-carbonate (C-C) coordination number, which is 12-fold in all of the carbonate liquids (Tissen and Janssen, 1990; Vuilleumier et al., 2014). The low-temperature monoclinic structures for the crystalline alkali carbonates and orthorhombic structures for the crystalline alkaline-earth carbonates all have C-C coordination numbers of 1 or 2. At high temperature the alkali carbonate structure (e.g., $P6_3/mmc$ for Na_2CO_3) has a C-C coordination number of ~6 whereas the alkaline-earth carbonate structure (e.g., $R\bar{3}m$) has a C-C coordination number of ~12, similar to that of the liquid. At even higher temperature (>1250 K), the structure for $BaCO_3$ becomes cubic (*Fm3m;* Strømme, 1975; Nie et al., 2017) and the C-C coordination of 12 is maintained. Thus with increasing temperature, the crystalline phase of $BaCO_3$

Table 7
Partial molar liquid volumes and crystalline volumes (with space groups).

	V^{liq}_{1100K} (cm^3/mol)	V^{xtl}_{298K} (cm^3/mol)	V_{liq}/V_{xtl} 298 K	V^{xtl}_{1100K} (cm^3/mol)	V_{liq}/V_{xtl} 1100 K
Li_2CO_3	41.22	35.20 $C2/c$[a]	1.17	37.03 C2/c[b]	1.11
Na_2CO_3	53.27	41.78 $C2/m$[c]	1.28	48.24 $P6_3/mmc$[d,e]	1.10
K_2CO_3	71.59	56.58 $P2_1/c$[f]	1.27	65.0 $P6_3/mmc$[g,h,i]	1.10
Rb_2CO_3	80.78	65.04 $P2_1/c$[j]	1.24	73.7 $P6_3/mmc$[i,*]	1.10
Cs_2CO_3	94.00	76.92 $P2_1/c$[j]	1.22	85.8 $P6_3/mmc$[i,*]	1.10
$CaCO_3$	40.18	34.18 $Pmcn$[k]	1.18	36.1 $Pmcn$[k]	1.11
		36.90 $R\bar{3}m$[l]	1.09	37.75 $R\bar{3}m$[m,n]	1.06
$SrCO_3$	44.33	38.98 $Pmcn$[o]	1.14	41.04 $Pmcn$[o]	1.08
				42.75 $R\bar{3}m$[p,q]	1.04
$BaCO_3$	50.99	45.73 $Pmcn$[o,r]	1.12	48.22 $Pmcn$[o,r]	1.06
				49.66 $R\bar{3}m$[o,p]	1.03
				49.70 $Fm\bar{3}m$[o]	1.03

[a] Effenberger and Zemann (1979).
[b] Liu and Lange (2003).
[c] Dusek et al. (2003).
[d] Swaison et al. (1995).
[e] Brouns and Visser (1964).
[f] Gatehouse and Lloyd (1973).
[g] Schneider and Levin (1973).
[h] Becht and Struikmans (1976).
[i] Dinnebier et al. (2005).
[j] Ehrhardt et al. (1980).
[k] Antao and Hassan (2010).
[l] Markgraf and Reeder (1985),
[m] Dove and Powell (1989).
[n] Antao and Hassan (2009).
[o] Nie et al. (2017).
[p] Lander (1949).
[q] Moreau (1964).
[r] Antao and Hassan (2007).
[*] Value extrapolated up to 1100 K from high-temperature data.

has a structure that is increasingly similar to the average structure of its corresponding liquid. The fact that all of the alkali and alkaline-earth carbonate liquids, irrespective of their M-O and M-C coordination numbers, have a shared and constant C-C coordination number of 12 may explain why the alkali and alkaline-earth liquid carbonate components all mix ideally with each other with respect to volume.

4.2. Systematic trends of carbonate liquid volume with cation coordination

The partial molar volumes (at 1100 K) of the liquid carbonate components are plotted as a function of cation field strength in Fig. 7. Cation field strength is defined as $z/(0.126 + r)^2$, where z is the formal cation charge, r is the crystalline ionic radius of the cation (Shannon and Prewitt, 1969; Shannon, 1976) and the 0.126 term is the ionic radius of the oxygen anion. The ionic radius of the cation depends on its coordination number with oxygen (M-O coordination number). For example, for alkali carbonate liquids, molecular dynamic simulations of Li_2CO_3, Na_2CO_3 and K_2CO_3 point to an oxygen coordination of ~4, ~5 and ~6 for Li^+, Na^+ and K^+, respectively (e.g. Habasaki, 1990; Tissen and Janssen, 1990; Roest et al., 2017). The ~4-fold coordination of Li-O in Li_2CO_3 liquid has been corroborated by neutron diffraction and XRD studies (Kohara et al., 1999). For alkaline earth carbonate liquids, molecular dynamic simulations show an average oxygen coordination of 7-fold for Ca^{2+} and Sr^{2+} and 8-fold for Ba^{2+} at 1 bar (Hurt, 2018). These results are consistent with first principle molecular dynamics simulations of $CaCO_3$ melt (Vuilleumier et al., 2014), which shows Ca^{2+} cations are 7- to 8-fold coordinated by oxygen at the higher pressure of ~0.5 GPa. Collectively, these 1-bar M-O coordination numbers for the alkali and alkaline earth metals are used to calculate their respective ionic radii and cation field strength (Table 9).

Plots of the liquid partial molar volume of each carbonate component as a function of field strength (Fig. 7) show two distinct trends, one for the alkali carbonate components (Li_2CO_3, Na_2CO_3, K_2CO_3, Rb_2CO_3 and Cs_2CO_3) and another for the alkaline earth carbonate components ($CaCO_3$, $SrCO_3$ and $BaCO_3$). The trend is curved for the alkali carbonate liquids, which cautions against a linear extrapolation of the alkaline earth carbonate trend to estimate the liquid partial molar volume for the $MgCO_3$ and $FeCO_3$ components.

In a second plot (Fig. 8), the partial molar volumes of all carbonate components are plotted as a function of cation volume (cm^3/mol), which is defined as $AvN4\pi r^3/3$ where Av is Avogadro's number, N is the stoichiometric number

Table 8
Coordination numbers of metal cations (i.e. Li, Na, K, Rb, Cs, Ca, Sr, Ba) with oxygen atoms (M-O), metal cations with carbonate groups (M-C) and carbonate groups with other carbonate groups (C-C) for low- and high-temperature crystal phases are compared to coordination numbers in their respective liquids.

	C-C	M-O	M-C
Li_2CO_3 $C2/c$[a]	2	4	4
Li_2CO_3 liquid[b]	12.5	3.7	3.8
Na_2CO_3 $C2/m$[c]	1	4.5	4
Na_2CO_3 $P6_3/mmc$[d]	5.9	6	5.5
Na_2CO_3 liquid[b]	12.6	5.2	4.2
K_2CO_3 $P2_1/c$[e]	2	4.5	5
K_2CO_3 Liquid[b]	12.0	6.0	4.4
$CaCO_3$ $Pmcn$[f]	2	9	6
$CaCO_3$ $R\bar{3}c$[g]	6	6	6
$CaCO_3$ $R3m$[h]	12	–	6
$CaCO_3$ liquid[i]	12	7.8	6
$SrCO_3$ $R\bar{3}m$[j]	12	–	6
$BaCO_3$ $R\bar{3}m$[k]	12	9	6
$BaCO_3$ $Fm3m$[j]	12	–	6

[a] Effenberger and Zemann (1979).
[b] Tissen and Janssen (1990).
[c] Arakcheeva et al. (2010).
[d] Swaison et al. (1995).
[e] Idemoto et al. (1998).
[f] Antao and Hassan (2010).
[g] Markgraf and Reeder (1985).
[h] Ishizawa et al. (2013).
[i] Vuilleumier et al. (2014).
[j] Strømme (1975).
[k] Antao and Hassan (2007).

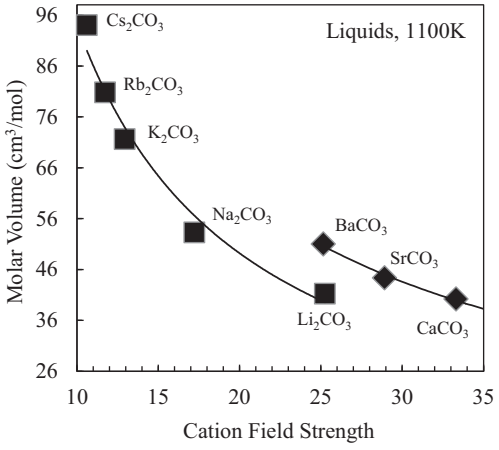

Fig. 7. Fitted liquid partial molar volume of each carbonate component at 1100 K (Table 5) as a function of cation field strength.

of cations per formula unit (2 for alkalis and 1 for alkaline earths) and r is the crystalline ionic radius. The results lead to two sub-parallel linear trends, with the alkali carbonate liquids falling on one line, and the alkaline-earth carbonate liquids on the other line. A linear fit to each set of liquids (Fig. 8) leads to the following equations, both with $R^2 = 0.999$:

$$V_{carbonate(alkali)} = 1.86(\pm0.03) \cdot V_{cation} + 38.3(\pm0.6) \quad cm^3/mol \tag{6a}$$

$$V_{carbonate(alkalineearth)} = 2.08(\pm0.01) \cdot V_{cation} + 31.0(\pm0.1) \quad cm^3/mol \tag{6b}$$

In both Eqs. (6a) and (6b), $V_{carbonate}$ is the molar volume of the carbonate liquid and V_{cation} is the cation volume as defined above. Table 9 lists the calculated cation volumes and field strength for each component in addition to the M-O coordination number and ionic radii. The slope intercepts of 38.3 (±0.6) and 31.0 (±0.1) cm^3/mol are fitted values (±1σ) for the partial molar volume of the carbonate ion, $(CO_3)^{2-}$, at 1100 K.

Importantly, the larger partial molar volume of $(CO_3)^{2-}$ in the alkali vs. alkaline earth carbonate liquids is not caused by a larger size for the carbonate ion. This is demonstrably not the case, as C—O distances (a proxy for the size of the carbonate molecule) in alkali carbonate liquids are not appreciably larger than in alkaline earth carbonate liquids. For example, Vuilleumier et al. (2014) and Hurt (2018) report C—O bond lengths in alkaline earth carbonate liquids of 1.29 Å (which, as Vuilleumier points out, is essentially the same as in calcite and aragonite). Roest et al. (2017), in their MD simulations, fixed C—O distances at 1.27 Å for alkali carbonate liquids. Instead, the difference in the partial molar volume of the carbonate ion reflects a systematic difference in the coordination of the various metal cations to the carbonate ions (M-C coordination number). For example, in the alkali carbonate liquids, the alkali metals are in a four-fold coordination with carbonate ions (e.g., Habasaki, 1990; Tissen and Janssen, 1990; Kohara et al., 1999; Roest et al., 2017), whereas in the alkaline earth carbonate liquids, the alkaline earth metals are all in a six-fold coordination with carbonate ions (Vuilleumier et al., 2014; Hurt, 2018). When the M-C coordination is four, this leads to a more open arrangement of the carbonate ions, and thus a larger partial molar volume (~38.3 cm^3/mole at 1100 K), in comparison to the case when the M-C coordination is six, leading to a more compact topology, and thus a smaller partial molar volume (~31.0 cm^3/mole at 1100 K).

An analogy can be drawn with 1-bar crystalline polymorphs of SiO_2, all of which are based on silica tetrahedra (Si^{4+} that is 4-fold coordinated by oxygen). The size of the silica tetrahedra does not change among the crystalline polymorphs (e.g., Stixrude and Bukowinski, 1988), but the way the tetrahedra are arranged into different ring structures (i.e., network topology) varies significantly (e.g., 6-membered rings in tridymite; 6- and 3-membered rings in quartz), leading to very different molar volumes at similar T-P conditions (e.g., Stixrude and Bukowinski, 1990).

4.3. Estimates of the partial molar volume of the liquid $MgCO_3$ and $FeCO_3$ components

If it is assumed that both Mg^{2+} and Fe^{2+} are six-fold coordinated by oxygen (slightly lower than the 7-fold coordination inferred for Ca^{2+}, given their smaller size) and six-

Table 9
Crystal radius, cation volume and cation field strength for each carbonate component.

Component	M-O coordination	Crystal radius (pm)	Cation volume (cm^3/mol)	Cation field strength
Li_2CO_3	4[a]	73	1.96	25.3
Na_2CO_3	5[a]	115	7.58	17.2
K_2CO_3	6[a]	152	17.7	12.9
Rb_2CO_3	6	166	23.1	11.7
Cs_2CO_3	6	181	29.9	10.6
$MgCO_3$[c]	6	86	1.60	44.5
	4	71	0.90	51.5
$CaCO_3$	7[b]	119	4.39	33.3
$SrCO_3$	7	137	6.36	28.9
$BaCO_3$	8	156	9.58	25.2
$FeCO_3$[c]	6	92	1.96	42.1
	4	77	1.15	48.5

[a] Tissen and Janssen (1990).
[b] Vuilleumier et al. (2014).
[c] Two sets of values are shown depending on an M-O coordination of 6 or 4.

fold coordinated by carbonate (similar to the case for Ca^{2+}, Sr^{2+} and Ba^{2+}), their cation volumes can be calculated and input into Eq. (6b), resulting in partial molar volumes of 34.4 ± 0.1 and 35.1 ± 0.1 cm^3/mol (Fig. 9), respectively, for the liquid $MgCO_3$ and $FeCO_3$ components. Note that if Mg^{2+} and/or Fe^{2+} are 4-fold (vs. 6-fold) coordinated by oxygen (similar to the case for Li^+ relative to K^+) this leads to smaller ionic radii, smaller cation volumes and smaller partial molar carbonate volumes. However, if Mg^{2+} and/or Fe^{2+} are 4-fold (vs. 6-fold) coordinated by carbonate, then the equation to use is Eq. (6a) (not (6b)), which leads to larger calculated partial molar volumes (40.1 ± 0.1 and 40.4 ± 0.1 cm^3/mol for $MgCO_3$ and $FeCO_3$ liquid respectively).

4.4. Comparison to estimates of liquid V_{MgCO3} and V_{FeCO3} from the literature

Dobson et al. (1996) measured the density of $K_2Mg(CO_3)_2$ liquid density at 773 and 837 K, using the single double-bob Archimedean method, using a corundum bob (~0.5 g) with a Pd wire stem (0.1 mm). They used the same approach to measure the density of $K_2Ca(CO_3)_2$ liquid between 1115 and 1249 K, which was directly compared to Pt double-bob density measurements on the same liquid in Liu and Lange (2003). There is a difference of ~3% in the results, with the corundum single-bob method leading to lower density determinations than those from the Pt double-bob method (Liu and Lange, 2003). Error analysis shows that because of the small mass of the corundum bob (~0.5 g) relative to that for Pt bobs (≤26 g), the estimated uncertainty in density using the corundum bob is ~2.5% (Liu and Lange, 2003). With this caveat in mind, an estimate of the partial molar volume of $MgCO_3$ obtained from the two Dobson et al. (1996) density measurements on $K_2Mg(CO_3)_2$ liquid can be made by incorporating them one by one into a fit of Eq. (4), combined with

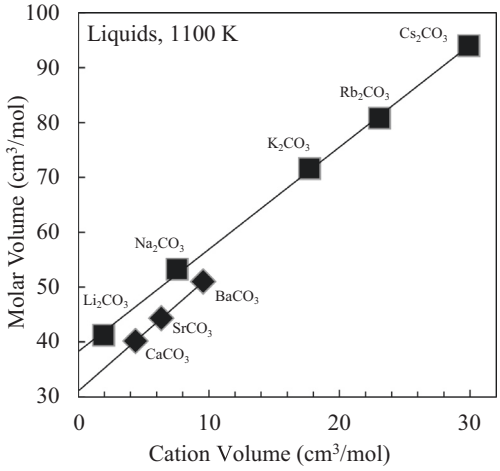

Fig. 8. Fitted liquid partial molar volume of each carbonate component at 1100 K (Table 5) as a function of cation field strength as a function of cation volume.

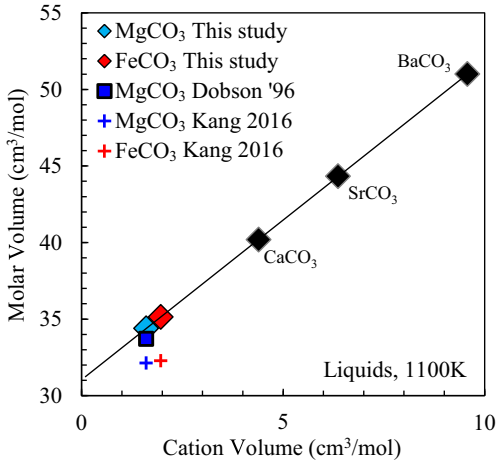

Fig. 9. Fitted liquid partial molar volumes of alkaline earth carbonate components at 1100 K (Table 5) as a function of cation volume together with estimates of liquid partial molar volume of $MgCO_3$ from data of Dobson et al. (1996) and Kang et al. (2016) and $FeCO_3$ from data of Kang et al. (2016). The cation volumes for Mg^{2+} and Fe^{2+} assume 6-fold M-O coordination.

all the Pt double-bob density results from this study and Liu and Lange (2003). The results lead to estimated $\bar{V}_{MgCO3}$ values of 31.87 and 32.31 cm^3/mole at 773 and 837 K, respectively. Use of the thermal expansion coefficient of 16.4 (±2.3) 10^{-5} K^{-1} (i.e., that for the alkaline-earth carbonate liquids; Fig. 5) leads to a molar volume of 33.7 cm^3/mol at 1100 K which overlaps within ±2.5% uncertainty the estimated value for V_{MgCO3} on the basis of Eq. (6b) (based on 6-fold M-O and M-C coordination). In contrast, this relatively low V_{MgCO3} (33.7 cm^3/mol) derived from Dobson's experiments is inconsistent with estimates calculated by Eq. (6a) (40.1 ± 0.1 cm^3/mol, which assumes a 4-fold M-O and M-C coordination). However, such an inconsistency does not rule out the possibility of 4-fold M-O and M-C coordination in $MgCO_3$ liquid since the composition explored by Dobson, $K_2Mg(CO_3)_2$, is

highly unusual. It is both the only $MgCO_3$-bearing liquid that is stable at 1 bar (e.g., Ragone et al., 1966) and the only purely carbonate liquid that quenches to a glass (e.g., Datta et al. 1964; Ragone et al. 1966). The unique properties of $K_2Mg(CO_3)_2$ may be a reflection of a unique liquid structure that is generally unrepresentative of the $MgCO_3$ liquid component in natural systems. This is exemplified in Mg-bearing silicate liquids where the average oxygen coordination of Mg^{2+} depends on the field strength of competing modifier cations (e.g., Ca^{2+}, Li^{+}, Na^{+}, K^{+}) in the melt (Shimoda et al., 2008).

The molar volumes and thermal expansion coefficients of liquid $MgCO_3$ and $FeCO_3$ have also been estimated by Kang et al. (2015, 2016) respectively, by fitting thermodynamic properties to recover the fusion curves of $FeCO_3$ and $MgCO_3$. Their fitted values for the molar volume of liquid $MgCO_3$ and $FeCO_3$ (calculated at 1100 K) are 32.1 and 32.3 cm^3/mol, respectively, which are lower than those estimated from Eq. (6b) and may be indirect evidence that the Mg^{2+} and Fe^{2+} cations are in a lower than 6-fold M-O coordination in carbonate liquids. However, the thermal expansion coefficients for the $MgCO_3$ and $FeCO_3$ liquid components in Kang et al. (2016) are those of the crystalline magnesite and siderite phases, which are nearly three times smaller than the average ($\sim$16.4 10^{-5} K^{-1}) obtained in this study at 1100 K for the alkaline earth carbonate liquid components. The liquid phase is expected to have a higher thermal expansion coefficient than corresponding mineral phases, because of configurational contributions to thermal expansion that is related to the fact that liquids undergo continual breaking and re-forming of bonds, which permits access to different topologies and modes of expansion that are unavailable to solids (e.g., Richet and Neuville, 1992; Lange, 1997; Toplis and Richet, 2000). To resolve this issue, high-quality computational simulations of $MgCO_3$ and $FeCO_3$ liquids are needed to constrain their M-O and M-C coordination numbers.

4.5. Importance of accurate liquid $\bar{V}_{MgCO3}$ and $\bar{V}_{FeCO3}$ values for applications to the Earth

As illustrated in the above two sections, estimates of $\bar{V}_{MgCO3}$ and $\bar{V}_{FeCO3}$ are highly dependent on M-C and M-O coordination. If M-O and M-C are in 4-fold coordination the estimated molar volumes of $MgCO_3$ and $FeCO_3$ liquid are $\sim$16–17% higher than if the M-O and M-C pairs are in 6-fold (40.1 versus 34.4 cm^3/mol for $MgCO_{3\ liquid}$ and 40.4 versus 35.1 cm^3/mol for $FeCO_{3\ liquid}$, at 1 bar and 1100 K). This corresponds to a 14% decrease in $MgCO_3$ liquid density (2.45 versus 2.10 g/cm^3) and a 13% decrease in $FeCO_3$ liquid density (3.30 versus 2.87 g/cm^3) if M-O and M-C are in four-fold coordination compared to six-fold. Such a density contrast could hold important implications for the buoyancy of Mg and Fe-rich carbonatites in the mantle, and thus for long term storage of carbon in the mantle. This is especially true for ferrocarbonatites that, according to some workers (i.e., Kang and Schmidt, 2017), could be dense enough to stagnate or sink in some parts of the upper mantle. While the magnitude of the 1-bar density contrast (13%) in $FeCO_3$ liquid with Fe^{2+} in 4-fold vs. 6-fold coordination probably diminishes with pressure, it may nonetheless be sufficiently large that it leads to a significant barrier to $FeCO_3$-rich liquids from achieving neutral or negative buoyancy in the upper-mantle. Knowledge of the liquid compressibility of these two components, therefore, and how it changes with pressure, is required before this issue can be fully explored and resolved.

It is also possible that the actual coordination of Mg^{2+} and Fe^{2+} is a non-integer value intermediate between 4- and 6-fold. The key point is that there is a need for high-quality computational simulations of $MgCO_3$ and $FeCO_3$ liquids to constrain their M-O and M-C coordination numbers, which will allow more accurate estimates of their respective liquid partial molar volumes from the linear trends in Fig. 8.

5. CONCLUSIONS AND FUTURE WORK

The results from this study show that multicomponent carbonate liquids mix ideally with respect to volume in the Li_2CO_3-Na_2CO_3-K_2CO_3-Rb_2CO_3-Cs_2CO_3-$CaCO_3$-$SrCO_3$-$BaCO_3$ system at 1 bar. Tight constraints on the partial molar volumes of the alkaline-earth carbonate components ($CaCO_3$, $SrCO_3$ and $BaCO_3$), which are not stable as pure liquids at one bar, are obtained by adding up to 50 mol% of each to the eutectic in the Li_2CO_3-Na_2CO_3-K_2CO_3 system, leading to multicomponent liquids that are stable at one bar over a wide range of temperature (758–1455 K). An area of future work is to extend this strategy to $MgCO_3$- and $FeCO_3$-bearing alkali carbonate liquids and to other thermodynamic property measurements, including 1-bar sound speeds to obtain melt compressibility (e.g., O'Leary et al., 2015) and 1-bar drop calorimetry to obtain the partial molar liquid enthalpies, heats of mixing, and partial molar liquid heat capacities for multicomponent carbonate liquids that include the alkaline-earth carbonate components.

Another key conclusion is that the partial molar volume of the carbonate ion depends on its coordination with the various alkali- and alkaline-earth metals. In this study, molecular dynamic simulations from the literature were used to constrain the oxygen coordination around the alkali and alkaline-earth metals in carbonate liquids, which controls the size of the ionic radius and thus the cation volume for each metal. When the liquid partial molar volumes of each respective carbonate component are plotted against their cation volumes, two distinct linear trends ($R^2 = 0.999$) result. The slope intercepts reflect two different partial molar volumes (and thermal expansion coefficients) for the carbonate ion, depending on its coordination with the respective alkali and alkaline-earth metals (i.e., the M-C coordination number). When the M-C is four-fold, both the partial molar volume ($\sim$38 cm^3/mol) and its thermal expansion coefficient ($\sim$22.1 10^{-5} K^{-1}) are larger than when the M-C is six-fold ($\sim$31 cm^3/mol and $\sim$ 16.4 10^{-5} K^{-1}, respectively). Fortunately, these differences do not preclude linear (ideal) mixing with respect to volume as long as the model equation employs carbonate components (and not oxide components with the carbonate ion). The reason why the liquid partial molar volumes mix ideally

at one bar is because all of the liquid carbonate components share the same carbonate-carbonate coordination number of 12, irrespective of their M-C and M-Ocoordination numbers.

The insights obtained in this study, when computational constraints on M-O and M-C coordination numbers are combined with macroscopic density measurements, show that accurate estimates of the partial molar volume and thermal expansion coefficient of the $MgCO_3$ and $FeCO_3$ components are possible if the M-C and M-Ocoordination numbers for Mg^{2+} and Fe^{2+} in carbonate melts can be obtained. This underscores the need for high-quality molecular dynamic simulations on $MgCO_3$- and $FeCO_3$-bearing carbonate melts in order to constrain the volumetric properties of these two relatively abundant carbonate components in the Earth's mantle. Knowledge of the standard state thermodynamic properties of these two important carbonate liquid components will allow thermodynamic models, such as p-MELTS (Ghiorso et al. 2002), to model partial melting of carbonate-bearing peridotite.

ACKNOWLEDGEMENTS

We thank the reviewers of this manuscript for their helpful and constructive feedback. We additionally thank Youxue Zhang, Aaron Wolf and Will Bender for their useful insights while writing this manuscript. Partial support for this research was provided from the National Science Foundation (NSF EAR-1763189), as well as the University of Michigan (Rackham Merit Fellowship to S.M. Hurt).

APPENDIX A

The molar volumes of crystal phases of each component have been collected from the literature and are shown as a function of temperature. The molar volume of the liquid is also shown as predicted by this study.

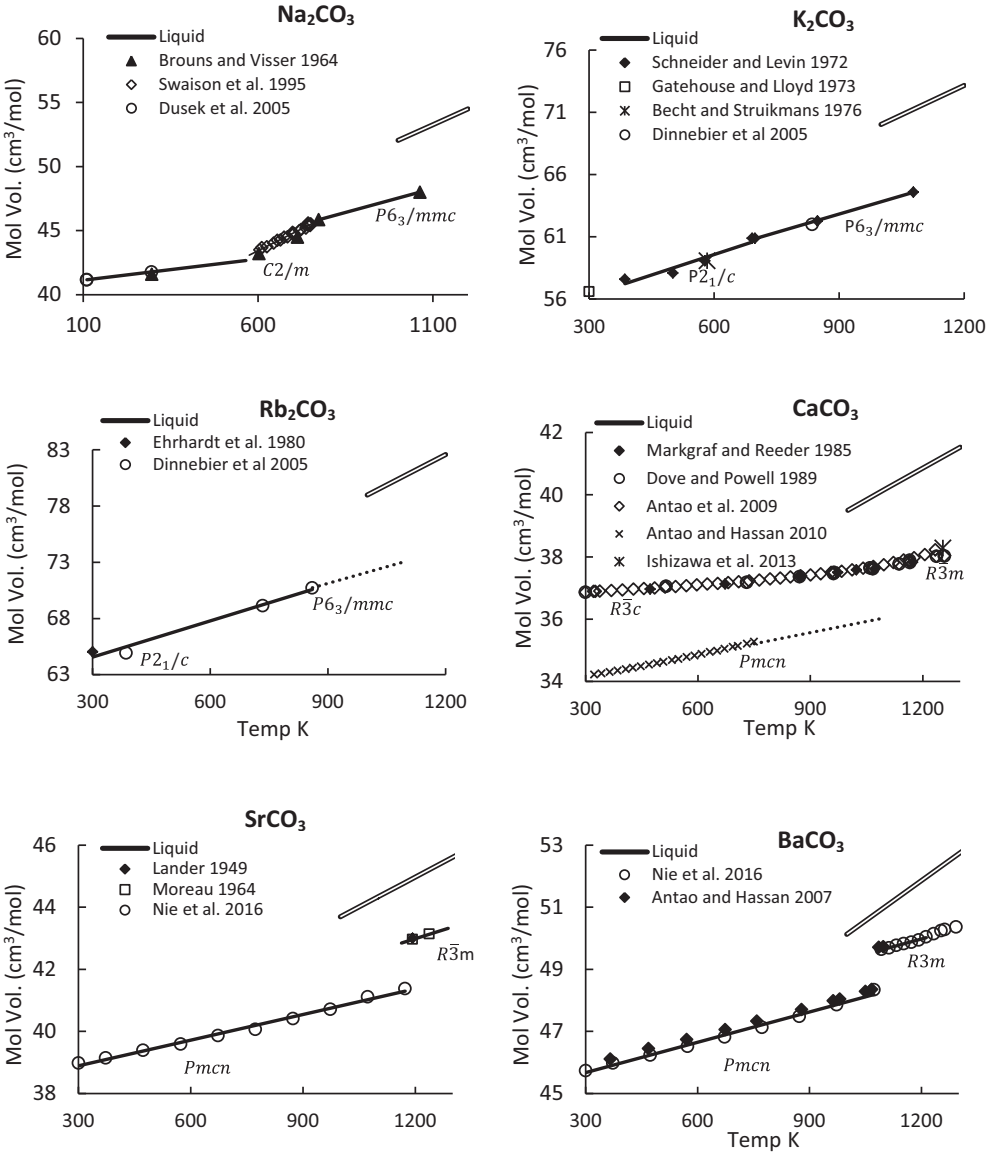

APPENDIX B. SUPPLEMENTARY MATERIAL

Supplementary data to this article can be found online at https://doi.org/10.1016/j.gca.2018.12.031.

REFERENCES

Antao S. M. and Hassan I. (2007) BaCO3: high-temperature crystal structures and the Pmcn→R3m phase transition at 811° C. *Phys. Chem. Miner.* **34**, 573–580.

Antao M. and Hassan I. (2009) The orthorhombic structure of $CaCO_3$, $SrCO_3$, $PbCO_3$ and $BaCO_3$: linear structural trends. *Can. Mineral.* **47**, 1245–1255.

Antao S. M. and Hassan I. (2010) Temperature dependence of the structural parameters in the transformation of aragonite to calcite, as determined from in situ synchrotron powder X-ray-diffraction data. *Can. Mineral.* **48**, 1225–1236.

Arakcheeva A., Bindi L., Pattison P., Meisser N., Chapuis G. and Pekov I. (2010) The incommensurately modulated structures of natural natrite at 120 and 293 K from synchrotron X-ray data. *Am. Min.* **95**, 574–581.

Becht H. Y. and Struikmans R. (1976) A monoclinic high-temperature modification of potassium carbonate. *Acta Cryst.* **B32**, 3344–3346.

Blundy J. and Dalton J. (2000) Experimental comparison of trace element partitioning between clinopyroxene and melt in carbonate and silicate systems, and implications for mantle metasomatism. *Contrib. Mineral. Petrol.* **139**, 356–371.

Brouns E. and Visser J. W. (1964) An anomaly in the crystal structure of Na_2CO_3. *Acta Cryst.* **17**, 614.

Cope E. R. and Dove M. T. (2007) Pair distribution functions calculated from interatomic potential models using the general utility lattice program. *J. Appl. Cryst.* **40**, 589–594.

Dalton J. A. and Wood B. J. (1993) The compositions of primary carbonate melts and their evolution through wallrock reaction in the mantle. *Earth Planet. Sci. Lett.* **119**, 511–525.

Dasgupta R. and Hirschmann M. M. (2006) Melting in the Earth's deep upper mantle caused by carbon dioxide. *Nature* **440**, 659–662.

Dasgupta R. and Hirschmann M. M. (2010) The deep carbon cycle and melting in Earth's interior. *Earth Planet. Sci. Lett.* **298**, 1–13.

Dasgupta R., Hirschmann M. M. and Stalker K. (2006) Immiscible transition from carbonate-rich to silicate-rich melts in the 3 GPa melting interval of eclogite + CO_2 and genesis of silica-undersaturated ocean island lavas. *J. Petrol.* **47**, 647–671.

Datta R. K., Roy D. M., Faile S. P. and Tuttle O. F. (1964) Glass formation in carbonate systems. *J. Am. Ceram. Soc.* **47**, 153.

Dinnebier R. E., Vensky S., Jansen M. and Hanson J. C. (2005) Crystal structures and topological aspects of the high-temperature phases and decomposition products of the alkali-metal oxalates $M_2[C_2O_4]$(M=K, Rb, Cs). *Chem Eur. J.* **11**, 1119–1129.

Dobson D. P., Jones A. P., Rabe R., Sekine T., Kurita K., Taniguchi T., Kondo T., Kato T., Shimomura O. and Urakawa S. (1996) In-situ measurement of viscosity and density of carbonate melts at high pressure. *Earth Planet. Sci. Lett.* **143**, 207–215.

Dove M. T. and Powell B. M. (1989) Neutron diffraction study of the tricritical orientational order/disorder phase transition in calcite at 1260 K. *Phys. Chem. Miner.* **16**, 503–507.

Dusek M., Chapuis G., Meyer M. and Petricek V. (2003) Sodium carbonate revisited. *Acta Cryst.* **B59**, 337–352.

Effenberger H. and Zemann J. (1979) Verfeinerung der kristallstruktur des lithiumkarbonates, Li_2CO_3. *Z. Kristallogr. Cryst. Mater.* **150**, 133–138.

Ehrhardt V. H., Schweer H. and Seidel H. (1980) Hochdrucksynthesen einiger carbonate mit überkristiischem CO_2. *Z. Anorg. Allg. Chem.* **462**, 185–198.

Gale J. D. and Rohl A. L. (2003) The General Utility Lattice Program (GULP). *Mol. Simul.* **29**, 291–341.

Gatehouse B. M. and Lloyd D. J. (1973) Crystal structure of anhydrous potassium carbonate. *J. Chem. Soc Dalton Trans.*, 70–72.

Ghiorso M. S., Hirschmann M. M., Reiners P. W. and Kress V. C. (2002) The pMELTS: a revision of MELTS for improved calculation of phase relations and major element partitioning related to partial melting of the mantle to 3 GPa. *Geochem. Geophys. Geosystems* **3**, 36.

Guo X., Lange R. A. and Ai Y. (2013) The density and compressibility of CaO-FeO-SiO_2 liquids at one bar: Evidence for four-coordinated Fe^{2+} in the $CaFeO_2$ component. *Geochim. Cosmochim. Acta* **120**, 206–219.

Habasaki J. (1990) Molecular dynamics simulation of molten Li_2CO_3 and Na_2CO_3. *Mol. Phys.* **69**, 115–128.

Hurt S. (2018) *The thermodynamic properties and structure and alkali and alkaline earth carbonate melts* Ph. D. thesis. Univ. Michigan.

Idemoto Y., Richardson J. W., Koura N., Kohara S. and Loong C. K. (1998) Crystal structure of $(Li_xK_{1-x})_2CO_3$ (x = 0, 0.43, 0.5, 0.62, 1) by neutron powder diffraction analysis. *J. Chem. Phys. Solids* **59**, 363–376.

Ishizawa N., Setoguchi H. and Yanagisawa K. (2013) Structural evolution of calcite at high temperatures: Phase V unveiled. *Sci. Rep.* **3**, 2832.

Kang N., Schmidt M. W., Poli S., Franzolin E. and Connolly J. A. D. (2015) Melting of siderite to 20 GPa and thermodynamic properties of $FeCO_3$-melt. *Chem. Geol.* **400**, 34–43.

Kang N., Schmidt M. W., Poli S., Connolly J. A. D. and Franzolin E. (2016) Melting relations in the system $FeCO_3$-$MgCO_3$ and thermodynamic modelling of Fe-Mg carbonate melts. *Contrib. Mineral. Petrol.* **171**, 1–16.

Kohara S., Suzuya K. and Ohno H. (1999) A reverse Monte Carlo study of molten lithium carbonate. *Plasmas Ions* **2**, 79–83.

Kojima T., Yanagida M., Tanimoto K., Tamiya Y., Matsumoto H. and Miyazaki Y. (1999) The surface tension and the density of molten binary alkali carbonate systems. *Electrochemistry* **67**, 593–602.

Kojima T., Miyazaki Y., Nomura K. and Tanimoto K. (2003) Density, molar volume, and surface tension of molten Li_2CO_3-Na_2CO_3 and Li_2CO_3-K_2CO_3 containing alkaline earth (Ca, Sr, and Ba) carbonates. *J. Electrochem. Soc.* **150**, E535–E542.

Kojima T., Miyazaki Y., Nomura K. and Tanimoto K. (2008) Density, surface tension, and electrical conductivity of ternary molten carbonate system Li_2CO_3-Na_2CO_3-K_2CO_3 and methods for their estimation. *J. Electrochem. Soc.* **155**, F150.

Lander J. J. (1949) Polymorphism and anion rotational disorder in the alkaline earth carbonates. *J. Chem. Phys.* **17**, 892–901.

Lange R. A. (1997) A revised model for the density and thermal expansivity of K_2O-Na_2O-CaO-MgO-Al_2O_3-SiO_2 liquids from 700 to 1900 K: extension to crustal magmatic temperatures. *Contrib. Mineral. Petrol.* **130**, 1–11.

Lange R. A. and Carmichael I. S. E. (1987) Densities of Na_2O-K_2O-CaO-MgO-FeO-Fe_2O_3-Al_2O_3-TiO_2-SiO_2 liquids: New measurements and derived partial molar properties. *Geochim. Cosmochim. Acta* **51**, 2931–2946.

Liu Q. and Lange R. A. (2001) The partial molar volume and thermal expansivity of TiO_2 in alkali silicate melts: Systematic variation with Ti coordination. *Geochim. Cosmochim. Acta* **65**, 2379–2393.

Liu Q. and Lange R. A. (2003) New density measurements on carbonate liquids and the partial molar volume of the $CaCO_3$ component. *Contrib. Mineral. Petrol.* **146**, 370–381.

Liu Q. and Lange R. A. (2006) The partial molar volume of Fe_2O_3 in alkali silicate melts: evidence for an average Fe^{3+} coordination number near five. *Am. Mineral* **91**, 385–393.

Markgraf S. and Reeder R. (1985) High-temperature structure refinements of calcite and magnesite. *Am. Miner.* **70**, 590–600.

Moreau R. (1964) Etude diffractometrique du carbonate de strontium et du carbonate de baryum entre 20 et 1000°C. *Bull. Soc. Franc. Miner. Crist.* **87**, 547–552.

Nie S., Liu Y., Liu Q., Wang M. and Wang H. (2017) Phase transitions and thermal expansion of $BaCO_3$ and $SrCO_3$ up to 1413 K. *Eur. J. Mineral.* **29**, 1–11.

O'Leary M. C., Lange R. A. and Ai Y. (2015) The compressibility of $CaCO_3$-Li_2CO_3-Na_2CO_3-K_2CO_3 liquids: Application to natrocarbonatite and CO_2-bearing nephelinite liquids from Oldoinyo Lengai. *Contrib. Mineral. Petrol.* **170**, 1–18.

Ragone S. E., Datta R. K., Roy D. M. and Tuttle O. F. (1966) The system potassium carbonate-magnesium carbonate. *J. Phys. Chem.* **70**, 3360–3361.

Richet P. and Neuville D. R. (1992) Thermodynamics of silicate melts: configurational properties. *Adv. Phys. Geochem.* **10**, 132–160.

Roest D. L., Ballone P., Bedeaux D. and Kjelstrup S. (2017) Molecular dynamics simulations of metal/molten alkali carbonate interfaces. *J. Phys. Chem. C* **121**, 17827–17847.

Schneider S. J. and Levin E. M. (1973) Polymorphism of K_2CO_3. *J. Am. Ceram. Soc.* **56**, 218–219.

Shannon R. D. (1976) Revised effective ionic radii and systematic studies of interatomic distances in halides and chalcogenides. *Acta Cryst.* **A32**, 751–767.

Shannon R. D. and Prewitt C. T. (1969) Effective ionic radii in oxides and fluorides. *Acta Cryst.* **B25**, 925–946.

Shimoda K., Takahiro N. and Saito K. (2008) Local structure of magnesium in silicate glasses: a ^{25}Mg 3QMAS NMR study. *J. Phys. Chem. B* **112**, 6747–6752.

Stein D. J., Stebbins J. F. and Carmichael I. S. E. (1986) Density of molten sodium aluminosilicates. *J. Am. Ceram. Soc.* **69**, 396–399.

Stixrude L. and Bukowinski M. S. T. (1990) Rings, topology, and the density of tectosilicates. *Am. Mineral* **75**, 1159–1169.

Stixrude L. and Bukowinski M. S. T. (1988) Simple covalent potential models of tetrhedral SiO2: Applications to α-quartz and coesite at pressure. *Phys. Chem. Minerals* **16**, 199–206.

Strømme K. O. (1975) On the crystal structures of the high-temperature forms of strontium and barium carbonate and structurally related compounds. *Acta Chem. Scand.* **29**, 105–110.

Swaison I. P., Dove M. T. and Harris M. J. (1995) Neutron powder diffraction study of the ferroelastic phase transition and lattice melting in sodium carbonate, Na_2CO_3. *J. Phys.: Condens Matter* **7**, 4395–4417.

Tissen J. T. W. M. and Janssen G. J. M. (1990) Molecular-dynamics simulation of molten alkali carbonates. *Mol. Phys.* **71**, 413–426.

Toplis M. J. and Richet P. (2000) Equilibrium density and expansivity of silicate melts in the glass transition range. *Contrib. Mineral. Petrol.* **139**, 672–683.

Vuilleumier R., Seitsonen A., Sator N. and Guillot B. (2014) Structure, equation of state and transport properties of molten calcium carbonate ($CaCO_3$) by atomistic simulations. *Geochim. Cosmochim. Acta* **141**, 547–566.

Associate editor: Michael J. Toplis